

## Accepted Manuscript

Influence of heat treatment on the high temperature oxidation mechanisms of an Fe-TiCN cermet

P. Alvaredo, C. Abajo, S.A. Tsipas, E. Gordo

PII: S0925-8388(13)02985-X

DOI: <http://dx.doi.org/10.1016/j.jallcom.2013.12.009>

Reference: JALCOM 30070

To appear in:

Received Date: 3 October 2013

Revised Date: 29 November 2013

Accepted Date: 2 December 2013

Please cite this article as: P. Alvaredo, C. Abajo, S.A. Tsipas, E. Gordo, Influence of heat treatment on the high temperature oxidation mechanisms of an Fe-TiCN cermet, (2013), doi: <http://dx.doi.org/10.1016/j.jallcom.2013.12.009>

This is a PDF file of an unedited manuscript that has been accepted for publication. As a service to our customers we are providing this early version of the manuscript. The manuscript will undergo copyediting, typesetting, and review of the resulting proof before it is published in its final form. Please note that during the production process errors may be discovered which could affect the content, and all legal disclaimers that apply to the journal pertain.



## Influence of heat treatment on the high temperature oxidation mechanisms of an Fe-TiCN cermet

P. Alvaredo\*, C. Abajo, S.A. Tsipas, E. Gordo

University Carlos III Madrid. Avda. de la Universidad, 30, 28911 Leganés (Spain)

\*Corresponding author. [palvared@ing.uc3m.es](mailto:palvared@ing.uc3m.es) Tel: +34 91 624 9482 Fax: +34 91 624 9430

### Abstract

In this study, the oxidation behaviour of an iron matrix cermet containing 50 % vol. Ti(C,N) was investigated before and after heat treatment by oxidation tests performed in static air at temperatures between 500 °C and 1000 °C. The oxidation mechanism for this type of composite materials was established and it was found that the heat treated material presents lower mass gain than the as-sintered material at the early stages of the oxidation, due to the volatilization of oxides. The oxidation behaviour of the sintered cermet was compared to those obtained for two commercial materials used in the fabrication of cutting tools, a high-speed steel and a cemented carbide, revealing a higher oxidation resistance for the iron matrix cermet due to the formation of a self-protective layer during the oxidation process.

**Keywords:** Metal matrix composites, powder metallurgy, oxidation, kinetics, scanning electron microscopy (SEM), X-Ray diffraction.

### 1. Introduction

Cemented carbides, tool steels and cermets are among the materials used to produce cutting tools, with cemented carbides being the most commonly used. However, in recent years, there has been growing interest in finding alternative materials to conventional cemented carbides due to the high and fluctuating price of Co, which is a reflection of its low abundance as well as its toxicity [1]. In this respect, in 2011, WC-Co was included in the '12th Report on Carcinogens' of the US Department of Health & Human Services as one of 240 substances that may increase risk for cancer both as a powder and as a sintered material [2].

Ti(C,N)-based cermets could be a competitive alternative to conventional WC-Co because, although cermets show lower toughness, they present superiority over cemented carbides in terms of other properties such as hardness, wear resistance and oxidation resistance [3, 4]. However, the metallic matrices used in Ti(C,N)-based cermets are Ni and/or Co, which also show a risk of toxicity.

There are several studies [5-7] that propose the use of Fe as a metallic matrix for cermets, as it is non-toxic and cheaper than Co or Ni, with the additional advantage of being able to be hardened by heat treatment. The disadvantage observed in processing Fe-matrix cermets is their poor wettability on Ti(C,N) particles during sintering in the liquid phase, which can be improved by the addition of alloying elements and compounds such as Cr, Mo, Mo<sub>2</sub>C or W [8]. Thus, in the present work, the metallic matrix chosen was a high-speed steel, M2 grade, which contains W, Mo and Cr. These alloying elements enhance different properties of the cermets with respect to those of a plain Fe matrix: (1) W, Mo and Cr improve the wettability between phases during sintering; (2) W and Mo are carbide formers that increase the hard phase of the compound; and (3) Cr increases the oxidation resistance of the material.

The materials used to manufacture tools must possess certain characteristics required by a given application, such as oxidation resistance to withstand the high temperatures reached during operation. The literature reveals many studies regarding the oxidation resistance of cemented carbides at high temperatures [9-14], as well as some investigations related to the thermodynamic stability of Ti(C,N)-based cermets [15-17] with conventional matrices.

However, the studies related to Fe matrix composites are scarce. Nevertheless, it is worth mentioning the work of Wittmann [6], who compared the oxidation resistance of a cemented carbide with that of a conventional Co matrix and that of an Fe matrix; and the study by Gómez [18], who studied the oxidation resistance of an M2-Ti(C,N) cermet, demonstrating the superior oxidation behaviour of the Ti(C,N) cermet with respect to that of the base material M2.

The present work extends the investigation carried out by Gómez by studying the effect of heat treatment on the oxidation behaviour of the same cermet. This study was motivated by the fact that the hardness of the heat-treated cermet increases by 25 % compared to that of the sintered one, and the fracture toughness also improves by 40 % [19]; therefore, it is necessary to study to what extent the metallurgical changes leading to the improved mechanical properties affect the oxidation behaviour of cermet. A comparison of the oxidation resistance of the sintered M2-Ti(C,N) cermet with that of two commercial materials used in the cutting tool industry, a cemented carbide and a high-speed steel, was also conducted.

## **2. Materials and experimental procedure.**

The composite material studied is composed of a high-speed steel, M2 grade, as the matrix and 50 vol% particles of Ti(C<sub>0.5</sub>N<sub>0.5</sub>) as a reinforcement. The composition of the M2 steel was 6.2 wt. % W, 4.8 wt. % Mo, 4.1 wt. % Cr, 1.8 wt. % V, 0.85 wt. % C and Fe balance; 0.5 wt.

% of graphite was also added. The density and particle size of the starting powders are given in Table 1.

Table 1: Characteristics of raw materials.

The samples were prepared by the conventional powder metallurgy route. Powders were mixed for 4 hours in a Turbula® mixer and then pressed in a uniaxial die at 750 MPa to obtain cylinders measuring 16 mm in diameter and 5 mm in height. The green compacts were sintered in vacuum ( $10^{-4}$  mbar) at 1400 °C for 60 minutes. The sintered materials were submitted to heat treatments similar to those normally applied to the high-speed steel used for the matrix, that is, austenitising at 1200 °C for 60 min under an Ar atmosphere, quenching in oil and double tempering at 560 °C for 60 minutes. The optimal conditions of the treatment were determined in a previous study in which other temperatures and times were studied [20]. Both as-sintered and heat-treated samples were characterised by scanning electron microscopy (SEM) and X-ray diffraction (XRD), and hardness was also measured as the control parameter of the heat treatment.

Isothermal oxidation tests were conducted in a muffle furnace in static air under different conditions: (1) The time was varied (12, 24, 48, 72 and 120 hours) at a fixed temperature (1000 °C) to study the oxidation kinetics. Samples of the M2-Ti(C,N) cermet in both the as-sintered condition and after the heat treatment were tested. The surface of all of the samples was prepared in the same way, by sequentially grinding with silicon carbide (SiC) abrasive papers up to 1000 grit. The samples were introduced into the furnace chamber, maintained at the predetermined temperature for the specified time and were taken out once the holding time at the temperature was reached. (2) The temperature (500 °C, 800 °C, and 1000 °C) was varied over a fixed time of 120 h. Samples of the M2-Ti(C,N) cermet and samples of commercial materials were submitted to these conditions. The commercial materials were used as a reference for the behaviour of the cermet under study, and for this purpose, a high-speed steel (M2 grade) and a cemented carbide (WC-10Co) were chosen.

In all cases, the samples were placed into the furnace in alumina crucibles and maintained under the selected conditions of the experiment. After the experiment, the mass was measured to calculate the change in mass per unit area. To study the microstructure and composition of the oxide scales, the samples were cut perpendicularly to the surface and the cross-section analysed by SEM and energy dispersive X-ray spectroscopy (EDX). As three different layers were observed by SEM, they were also analysed by XRD to determine the oxides present. The XRD analyses were performed on the surface of the samples, carefully removing the top layer after the analysis by polishing to expose and analyse the next layer. The free energy of formation of different oxides was calculated using the software HSC 4.1.

Thermodynamic calculations of the oxide scales formed in the M2-Ti(C,N) cermet during isothermal oxidation at 1000 °C were conducted using the Thermo-Calc software with the SSUB4 database [21].

### 3. Results and discussion.

#### 3.1. Characterisation of the as-sintered and heat-treated M2-Ti(CN) cermet

Figure 1 shows SEM images of the microstructure of the as-sintered and the heat-treated M2-Ti(C,N) cermet. Both microstructures present three different phases: the dark phase corresponds to Ti(C,N) particles, the grey phase corresponds to the steel matrix and the third bright phase corresponds to the carbides of the alloying elements (W, Mo and V) from the high-speed steel matrix. Although the microstructures present the same three main phases, the heat-treated sample shows a hardness increase of 25 % with respect to the hardness of the as-sintered sample. Therefore, the steel matrix could be composed of different phases after the heat treatment. Figure 2 shows the results of the XRD analysis performed on the sintered and heat-treated cermets.

Figure 1. Microstructures (SEM images) of M2-Ti(C,N) cermets: a) as-sintered and b) heat-treated.

The diffractograms of both samples present peaks corresponding to the Ti(C,N) particles, peaks corresponding to the ferrite (Fe- $\alpha$ ) or martensite in the steel matrix (note that the XRD patterns of ferrite and martensite are quite similar, and thus, it was not possible to distinguish them in this analysis) and peaks corresponding to carbides of the alloying elements of the steel matrix, mainly MC type carbide rich in V, Mo and W and M<sub>2</sub>C carbide rich in Mo and W, both typical in high speed steels. That is, the XRD analyses confirm the presence of the three main phases already observed in the microstructures but also highlight the main difference between the as-sintered and heat-treated cermet, namely, the presence of austenite phase (Fe- $\gamma$ ) in the sintered cermet, which does not appear in the heat-treated one. This result could be explained by the transformations that take place during heat treatment. During the austenitising step, the carbides of alloying elements from the high-speed steel are dissolved in the iron matrix, increasing the concentration of carbon and alloying elements in the matrix and stabilising the austenite such that, after quenching, the microstructure would contain retained austenite enriched with alloying elements, together with martensite. The increase of in temperature during the first tempering favours the diffusion of the alloying elements outside the austenite and leads to the formation of secondary carbides and martensite. In the second tempering, the retained austenite transforms completely, and

consequently, the austenite phase (Fe- $\gamma$ ) is not present in the XRD pattern of the heat-treated sample. The final quantity of the carbides after the double tempering is lower than that in the as-sintered sample, as demonstrated in the microstructures shown in Figure 1, meaning that part of the alloying elements remains dissolved in the iron matrix. It is important to take this fact into account because it is one of the factors affecting the different oxidation behaviour of the as-sintered and heat-treated materials.

Figure 2. Results of X-Ray diffraction analysis of the as-sintered and heat-treated M2-Ti(C,N) cermets.

### 3.2. Oxidation kinetics of as-sintered and heat-treated M2-Ti(CN) cermets

The oxidation kinetics were determined by measuring the mass gain after the oxidation experiments carried out at 1000 °C for different exposure times: 12, 24, 48, 72 and 120 hours. In

Figure 3, the mass gain with respect to the exposure time of the sintered and heat-treated cermets is represented. The mass gain rate of the sintered sample at short exposure times is higher than the mass gain rate of the heat-treated one, whereas this behaviour is altered after an exposure time of 24 hours, as shown in Table 2. Thus, although the mass gain of the sintered sample is higher at early stages of the oxidation test, the final mass gain of the as-sintered cermet after 120 hours of exposure is 150 mg/cm<sup>2</sup> and that of the heat-treated one under the same oxidation conditions is slightly higher, 166.9 mg/cm<sup>2</sup>. Beyond 12 h, the oxidation kinetic of the sintered cermet follows a logarithmic trend, Eq. (1), and the oxidation kinetic of the heat-treated cermet follows a linear trend, Eq. (2).

$$y = 41.044\ln(x) + 46.455; R^2 = 0.9997 \quad (1)$$

$$y = 1.1803x + 26.368; R^2 = 0.9962 \quad (2)$$

where  $y$  represents the mass gain (mg/cm<sup>2</sup>) and  $x$  represents the exposure time (hours).

Figure 3. Mass gain with respect to the exposure time in oxidation tests performed at 1000 °C of the as-sintered and heat-treated M2-Ti(C,N) cermets. (Experiments in furnace).

Table 2. Mass gain rate for sintered and heat-treated samples for each exposure time range.

### 3.3. Characterisation of oxide scales of as-sintered and heat-treated M2-Ti(C,N) cermet

Figure 4 shows cross-sections of the as-sintered and heat-treated M2-Ti(C,N) cermets after the oxidation experiment performed in a furnace at 1000 °C for 120 hours. In both samples, the oxidation surface presents three different layers. The outer one is porous and has a thickness of approximately 150  $\mu$ m; the intermediate layer is approximately 500  $\mu$ m thick with coarser pores than the outer one; and the inner layer is compact and approximately 200  $\mu$ m

in thickness. The main difference between the two materials is the higher number of cracks and pores in the inner layer of the heat-treated material in addition to a weaker bonding between layers than in the oxidation surface of the as-sintered cermet. The same figure shows SEM images at higher magnifications of the bulk material after the oxidation treatment. No significant differences are evident between the as-sintered and heat-treated materials, but some changes can be observed in the size and morphology of the carbides and Ti(C,N) particles in relation to the material before the oxidation tests, as expected.

Figure 4. SEM images (BSE mode) of the cross-sections of the a) as-sintered and b) heat-treated M2-Ti(C,N) cermets after the oxidation test performed at 1000 °C for 120 h. Detailed view of the bulk material after the oxidation experiment: c) as-sintered, d) heat-treated.

The oxides present in the oxidation layers were studied by XRD analysis and SEM-EDX, and the results are shown in Figure 5. For the sintered sample, the XRD analysis of the outer layer shows only one type of oxide,  $\text{Fe}_2\text{O}_3$ ; the analysis of the intermediate layer also shows the formation of  $\text{Fe}_2\text{O}_3$ , as well as  $\text{WO}_2$ ,  $\text{TiO}_2$  and  $\text{Mo}_3\text{O}$ , and the analysis of the inner layer, the compact one, shows the formation of  $\text{TiO}_2$ ,  $\text{Fe}_3\text{O}_4$  and  $\text{FeTiO}_3$ . The XRD and SEM-EDX analyses of the heat-treated samples reveal the same type of oxide in the outer layer,  $\text{Fe}_2\text{O}_3$ , but the analyses of the intermediate layer show  $\text{Fe}_2\text{O}_3$ ,  $\text{TiO}_2$  and a new oxide  $\text{Fe}_2\text{TiO}_5$ ; no Mo or W oxides were identified in this layer; the analysis of the inner layer shows the formation of the oxides  $\text{WO}_2$ ,  $\text{FeTiO}_3$  and  $\text{TiO}_2$ .

Figure 5. XRD analysis of the outer, intermediate and inner layers formed on the surface of the M2-Ti(C,N) cermets after the oxidation tests performed at 1000 °C for 120 h. a) As-sintered, b) heat-treated.

The composition of the oxidation layers was also analysed by EDX, and the results, presented in Figure 6, are in accordance with those obtained by XRD analysis. In the heat-treated material, the Fe content decreases in the inner layer and increases gradually from the intermediate layer to the outer one, whereas in the sintered material, the Fe content is lowest in the intermediate layer and highest in the outer layer. On the other hand, for the heat-treated sample, the highest Ti content is in the inner layer and decreases gradually towards the outer layer, whereas for the sintered sample, the Ti content is highest in the intermediate layer and lowest in the outer layer. Another important difference between the composition of the oxide layers of the sintered and heat-treated cermets is related to the W and Mo contents. As demonstrated in the XRD analysis, these elements are not present in the intermediate layer of the heat-treated cermet, whereas the highest content of the elements in the sintered cermet is found in the intermediate layer. Moreover, due to the

presence of  $\text{WO}_2$  in the inner layer of the heat-treated sample, the highest W content occurred in this layer.

Figure 6. EDX analysis of surface layers of as-sintered and heat-treated cermets.

### 3.4 Thermodynamic studies

A thermodynamic study was performed by calculating the stability of the main Fe and Ti oxides with respect to the temperature using the HSC 4.1 software program, and the mass fraction of those oxides as a function of the oxygen partial pressure was calculated using Thermocalc software.

In Figure 7, the Gibbs free energy as a function of the temperature for the reaction of Fe, TiC and TiN with one mol of oxygen is presented. The calculations show that the formation of  $\text{Fe}_2\text{O}_3$ ,  $\text{Fe}_3\text{O}_4$  and  $\text{TiO}_2$  is thermodynamically favourable and that the formation of the oxide  $\text{TiO}_2$  by the reaction of TiC and TiN with O shows the highest stability.

The formation of  $\text{Fe}_3\text{O}_4$  is more favourable than the formation of  $\text{Fe}_2\text{O}_3$  over the entire temperature range; nevertheless, the experimental analysis of the oxides revealed that the main iron oxide formed was  $\text{Fe}_2\text{O}_3$ . To understand the thermodynamic stability of the oxides, the mass fraction of the equilibrium phases with respect to the oxygen partial pressure was calculated as it has been performed in others works found on the literature [22], and it is shown in Figure 8. In this graph, only the mass phase fraction of the main oxides observed after the oxidation experiment is presented, namely,  $\text{TiO}_2$ ,  $\text{FeTiO}_3$ ,  $\text{Fe}_3\text{O}_4$  and  $\text{Fe}_2\text{O}_3$ , as a function of the oxygen partial pressure ( $P(\text{O}_2)$ ). The phases that appear at lower  $P(\text{O}_2)$  can be assumed to exist in the inner layer close to the bulk material, and the phases that appear at higher  $P(\text{O}_2)$  can be assumed to exist in the outer layer of the oxidation surface.

The results show that  $\text{TiO}_2$  and  $\text{FeTiO}_3$  appear at low  $P(\text{O}_2)$ , whereas the iron oxides appear at high  $P(\text{O}_2)$ , with  $\text{Fe}_2\text{O}_3$  phase appearing at the highest  $P(\text{O}_2)$ . These results are in accordance with the experimental results obtained for the case in which  $\text{Fe}_2\text{O}_3$  was observed in the outer oxide layer.

Figure 7. Gibbs free energy as a function of temperature of the possible oxides formed during oxidation experiments, calculated by the HSC 4.1 software program.

Figure 8. Phase fraction of a)  $\text{TiO}_2$ , b)  $\text{FeTiO}_3$ , c)  $\text{Fe}_2\text{O}_3$  and d)  $\text{Fe}_3\text{O}_4$  in the oxidation surface layers as a function of the oxygen partial pressure ( $P(\text{O}_2)$ ) calculated using Thermocalc software [21].

### 3.5. Oxidation surface morphology

Another difference observed when comparing the sintered and heat-treated cermets after the oxidation experiments performed in a furnace at 1000 °C for 120 h is their surface morphology, shown in Figure 9. The oxidation surface of the as-sintered cermet has a smooth morphology, in contrast with the surface morphology of the heat-treated cermet, which exhibits spheres growing on top of each to form a columnar shape. This morphology may indicate the escape of gases during the oxidation process.

Figure 9. Morphology of the oxidation surface of as-sintered and heat-treated M2-Ti(C,N) cermets after oxidation experiment performed at 1000 °C for 120 h in a muffle furnace.

### 3.6. Oxidation mechanism

Considering all of the results obtained, the oxidation mechanisms of the M2-Ti(C,N) cermet in the as-sintered and heat-treated conditions can be proposed.

The schematic diagram shown in Figure 10 depicts the oxidation mechanism proposed for the as-sintered cermet. The outer layer contains only  $\text{Fe}_2\text{O}_3$ , which is probably formed by the direct reaction of oxygen with the Fe of the steel matrix [22]. Due to the porous nature of this layer, the inward diffusion of oxygen is plausible. The intermediate layer contains reaction products formed by the reaction between oxygen and the steel matrix, as well as TiCN and carbide particles. Therefore, this layer is probably formed by the inward diffusion of oxygen, which reacts with both the Fe matrix and the Ti(C,N) particles to form  $\text{Fe}_2\text{O}_3$ ,  $\text{TiO}_2$ ,  $\text{WO}_2$  and  $\text{Mo}_3\text{O}$  oxides. This layer also appears to be permeable to oxygen. The inner layer is more compact and protective and composed of the stable oxides  $\text{TiO}_2$  and  $\text{FeTiO}_3$ , which could be formed by the inward diffusion of oxygen. According to the thermodynamic calculations, these oxides may be stable at lower oxygen partial pressures. It is interesting to note that oxides of W and Mo, even though they are volatile, are trapped in the intermediate layer. This is one of the differences observed with respect to the oxidation of the heat-treated samples, whose significance will be explained later.

This mechanism is in accordance with the oxidation kinetic law. During the early stages of oxidation, the mass gain rate is higher, and after the formation of the protective layer, the mass gain rate decreases.

Figure 10. Schematic diagram of the oxidation mechanism proposed for the as-sintered M2-Ti(C,N) cermet.

The schematic diagram shown in Figure 11 depicts the oxidation mechanism proposed for the heat-treated cermet. Similarly to the sintered material, the outer layer consisted of a porous layer of  $\text{Fe}_2\text{O}_3$ , probably formed by the direct reaction of oxygen with the Fe of the

steel matrix. In this case, the intermediate layer only contains  $\text{Fe}_2\text{O}_3$  and  $\text{TiO}_2$ , without the presence of  $\text{WO}_2$  and  $\text{Mo}_3\text{O}$  that appeared in the as-sintered material. On the other hand, the inner layer contains W oxides. The explanation for the differences encountered lies in the microstructural features and, in particular, in the distribution of the carbides of the alloying elements. In the case of the as-sintered material, the alloying elements W and Mo form carbides that are located mainly around the Ti(C,N) particles. In the case of the heat-treated material, the alloying elements are partially dissolved in the steel matrix or occur as very fine carbide precipitates, which are less stable than the primary carbides present in the as-sintered [23, 24]. Therefore, the alloying elements in the heat-treated material can react with directly with oxygen to form oxides, as opposed to what occurs in the as-sintered cermet, in which the oxygen has to react with the primary carbides instead of with the elements in solid solution. Due to the volatile nature of the oxides formed, they escape from the sample outwards, leaving the intermediate layer free of these oxides and leading to lower mass gain than as-sintered material during the early stages of the experiments, as well as an oxidation layer with more pores and cracks. A similar mechanism has been suggested by other researchers [12] where the generation of pores is associated with volatile oxides and cracks with stresses within the oxide scale. The inner layer, however, presents W oxides, probably trapped in the same manner observed during the formation of the intermediate layer in the as-sintered sample. The volatilisation of  $\text{WO}_2$  and  $\text{Mo}_3\text{O}$  may also be responsible for the surface morphology observed for the heat-treated sample, shown in Figure 9. This morphology has also been related to selective oxidation in another study [25].

Figure 11. Schematic diagram of the oxidation mechanism proposed for the heat-treated M2-Ti(C,N) cermet.

### 3.6. Comparison with commercial materials

To complete the study, the oxidation resistance of the M2-Ti(C,N) cermet was compared with the oxidation resistance of two commercial materials used in the fabrication of cutting tools, namely, a high-speed steel (M2 grade) and a cemented carbide.

Figure 12a shows the effect of temperature on samples of the three materials after oxidation tests performed at 500 °C, 800 °C and 1000 °C for 120 h. Figure 12b shows the mass gain of the materials with respect to the oxidation temperature after the oxidation experiments were performed in a muffle furnace.

At 500 °C, none of the samples studied exhibit geometric changes and the three materials show almost no mass change. However, after the oxidation tests at 800 °C, the commercial materials, high-speed steel (M2) and cemented carbide, show catastrophic oxidation, leading to a total disintegration of the material, whereas the cermet maintains its cylindrical shape.

This behaviour is in accordance with the mass gain results shown in Figure 12b. The mass gain of the commercial materials after the oxidation test performed at 800 °C is much higher than the mass gain of the sintered cermet, with the high-speed steel sample presenting the highest mass gain. After the oxidation experiment performed at 1000 °C for 120 h, the mass gains of the M2-Ti(C,N) cermet, the cemented carbide and the high-speed steel were 24.4, 162.5 and 334.5 mg/cm<sup>2</sup>, respectively. The mass gain of the commercial materials decreases drastically due to the liberation of volatile oxides formed, which promote the catastrophic oxidation and complete disintegration of the samples, as shown in Figure 12a. By comparing the oxidation behaviour of the commercial high-speed steel with that of the cermet, a lower mass gain of the composite material is observed. This discrepancy is observed because the presence of the Ti(C,N) particle reinforcement allows for the formation of a protective layer of TiO<sub>2</sub> and FeTiO<sub>3</sub>, which prevents the oxidation of the bulk material.

Figure 12. a) Samples of commercial M2 high-speed steel (left), commercial hard metal (centre) and sintered M2-Ti(C,N) cermet (right) after oxidation tests performed at 500 °C, 800 °C and 1000 °C for 120 h. b) Mass gain with respect to oxidation temperature during oxidation experiment performed in a muffle furnace for 120 h.

#### 4. Conclusions

A Ti(C,N) based cermet with Fe alloy as binder phase was prepared by powder metallurgy and subsequently heat treated by quenching in oil from 1200 °C and double tempering at 560 °C for 60 minutes. Materials as-sintered and heat treated were subjected to oxidation experiments at 1000 °C for different times up to 120 h in static air. The oxide scales were characterized to evaluate the oxidation mechanisms at high temperature and to understand the influence of the heat treatment. In both cases the oxide scales were multilayer, consisting of a protective inner layer of TiO<sub>2</sub> and FeTiO<sub>3</sub>, and an outer layer of Fe<sub>2</sub>O<sub>3</sub>. The main difference between the as-sintered and heat treated materials is the composition of the interlayer, which shows the presence of WO<sub>2</sub> and Mo<sub>3</sub>O in the as-sintered material, whereas these oxides are not found in the heat treated material. This difference is due to the heat treatment, during which the alloying elements are dissolved in the steel matrix or are present as very fine precipitates, which are less stable than the primary carbides found in the as-sintered cermet. This observation, together with the mass gain variation during the oxidation experiments, and the thermodynamic calculations permit to explain the differences found in the oxidation mechanisms: the heat treated material presents lower mass gain than the as-sintered material at the early stages of the oxidation, due to the volatilization of oxides. This leads to a quasi-linear trend in the mass gain kinetics for the heat treated material versus a logarithmic trend for the as-sintered.

The oxidation behavior of the as-sintered material was also compared to the behavior of two commercial tool materials: a high-speed steel and a cemented carbide. The superiority of the cermet in the conditions studied was demonstrated, and explained by the formation of a protective layer of  $\text{TiO}_2$  and  $\text{FeTiO}_3$  during the oxidation process.

## Acknowledgements

The authors acknowledge the funding received for this work from the Spanish Government through the R&D projects MAT2009-14448-C02-02 and MAT2012-38650-C02-01 and the Regional Government of Madrid through the ESTRUMAT program (S-2009/MAT-1585).

## References

- [1] P.L. Gries B., Acute inhalation toxicity by contact corrosion - the case of WC-Co, in: EPMA (Ed.) Proceedings EURO PM2007 Shrewsbury, 2007, pp. 189-196.
- [2] National Toxicology Program. Department of health and human services. <http://ntp.niehs.nih.gov/?objectid=03C9AF75-E1BF-FF40-DBA9EC0928DF8B15>, in, USA.
- [3] P. Ettmayer, H. Kolaska, W. Lengauer, K. Dreyer, Ti(C,N) cermets -- Metallurgy and properties, International Journal of Refractory Metals and Hard Materials, 13 (1995) 343-351.
- [4] A. Bellosi, R. Calzavarini, M.G. Faga, F. Monteverde, C. Zancolò, G.E. D'Errico, Characterisation and application of titanium carbonitride-based cutting tools, Journal of Materials Processing Technology, 143-144 (2003) 527-532.
- [5] E. Gordo, Gómez, B., Ruiz-Navas, E.M., Torralba, J.M., Influence of milling parameters on the manufacturing of Fe-TiCN composite powders, Journal of Materials Processing Technology 162-163 (2005) 59-64.
- [6] B. Wittmann, W.-D. Schubert, B. Lux, WC grain growth and grain growth inhibition in nickel and iron binder hardmetals, International Journal of Refractory Metals and Hard Materials, 20 (2002) 51-60.
- [7] G.B. Prakash L., WC hardmetals with Iron based binders, in: P.R. L. Sigl, H. Wildner (Ed.) Proceedings of 17th Plansee Seminar, Reutte (Austria), 2009, pp. HM 5/1- HM 5/13.
- [8] A.P. Umanskii, Titanium carbonitride composite with iron chromium binder, Powder Metallurgy and Metal Ceramics, 40 (2001) 637-640.
- [9] X. Shi, H. Yang, G. Shao, X. Duan, S. Wang, Oxidation of ultrafine-cemented carbide prepared from nanocrystalline WC-10Co composite powder, Ceramics International, 34 (2008) 2043-2049.
- [10] S.N. Basu, V.K. Sarin, Oxidation behavior of WC-Co, Materials Science and Engineering: A, 209 (1996) 206-212.
- [11] M. Aristizabal, J.M. Sanchez, N. Rodriguez, F. Ibarreta, R. Martinez, Comparison of the oxidation behaviour of WC-Co and WC-Ni-Co-Cr cemented carbides, Corrosion Science, 53 (2011) 2754-2760.
- [12] C. Barbatti, J. Garcia, P. Brito, A.R. Pyzalla, Influence of WC replacement by TiC and (Ta,Nb)C on the oxidation resistance of Co-based cemented carbides, International Journal of Refractory Metals and Hard Materials, 27 (2009) 768-776.
- [13] B.R. Bhaumik S. K., Upadhyaya G. S. ,Vaidya M. L. , Oxidation behaviour of hard and binder phase modified WC-10Co cemented carbides, Journal of Materials Science Letters, 11 (1992) 1457-1459.

- [14] V.B. Voitovich, V.V. Sverdel, R.F. Voitovich, E.I. Golovko, Oxidation of WC-Co, WC-Ni and WC-Co-Ni hard metals in the temperature range 500–800 °C, *International Journal of Refractory Metals and Hard Materials*, 14 (1996) 289-295.
- [15] F. Monteverde, A. Bellosi, Oxidation behavior of titanium carbonitride based materials, *Corrosion Science*, 44 (2002) 1967-1982.
- [16] Q. Yang, W. Xiong, S. Li, H. Dai, J. Li, Characterization of oxide scales to evaluate high temperature oxidation behavior of Ti(C,N)-based cermets in static air, *Journal of Alloys and Compounds*, 506 (2010) 461-467.
- [17] Q. Yang, W. Xiong, S. Li, Z. Yao, X. Chen, Early high temperature oxidation behaviour of Ti(C,N)-based cermets in air, *Corrosion Science*, 52 (2010) 3205-3211.
- [18] B. Gómez, A. Jiménez-Suarez, E. Gordo, Oxidation and tribological behaviour of an Fe-based MMC reinforced with TiCN particles, *International Journal of Refractory Metals and Hard Materials*, 27 (2009) 360-366.
- [19] J.A. Canteli, J.L. Cantero, N.C. Marín, B. Gómez, E. Gordo, M.H. Miguélez, Cutting performance of TiCN–HSS cermet in dry machining, *Journal of Materials Processing Technology*, 210 (2010) 122-128.
- [20] P. Alvaredo, Nuevos materiales tipo cermet matriz Fe: Estudio de composición, microestructura y propiedades, in: *Ciencia e Ingeniería de Materiales e Ingeniería Química*, Universidad Carlos III de Madrid, Madrid, 2012.
- [21] J.O. Andersson, T. Helander, L. Höglund, P. Shi, B. Sundman, Thermo-Calc & DICTRA, computational tools for materials science, *Calphad*, 26 (2002) 273-312.
- [22] H.H. Kim, J.W. Lim, J.J. Lee, Oxidation behavior of high-speed steels in dry and wet atmospheres, *Isij International*, 43 (2003) 1983-1988.
- [23] G. Schlieper, F. Thummler, High-strength heat-treatable sintered steels containing manganese, chromium, vanadium and molybdenum, *Powder Metallurgy International*, 11 (1979) 172-179.
- [24] Albanomu.L, F. Thummler, G. Zapf, High-strength sintered iron-based alloys by using transition-metal carbides, *Powder Metallurgy*, 16 (1973) 236-256.
- [25] A. Martínez-Villafañe, J.G. Chacon-Nava, C. Gaona-Tiburcio, F. Almeraya-Calderon, R. Bautista- argulis onzalez-Rodr guez, The effect of Nd and Pr on the oxidation behavior of a Fe–13Cr alloy, *Scripta Materialia*, 46 (2002) 127-130.

Table 1: Characteristics of raw materials.

Raw material	Supplier	Supplier data		Experimental data	
		Density (g/cm <sup>3</sup> )	Particle size (μm)	Density (g/cm <sup>3</sup> )	Particle size (μm)
Ti(C <sub>0.5</sub> N <sub>0.5</sub> )	H. C. Starck	5.03	D50 = 3.71	5.12	D50 = 3.96
HSS, M2	Osprey	8.58	D80<16	8.09	D50= 8.15

Table 2. Mass gain rate for sintered and heat treated samples for each exposure time range.

Exposure time (hours)	Sintered	Heat treated
	Mass gain rate (mg·cm <sup>-2</sup> /hour)	Mass gain rate (mg·cm <sup>-2</sup> /hour)
0-12	4.61	3.02
12-24	2.50	1.83
24-48	1.12	1.13
48-120	0.52	1.13

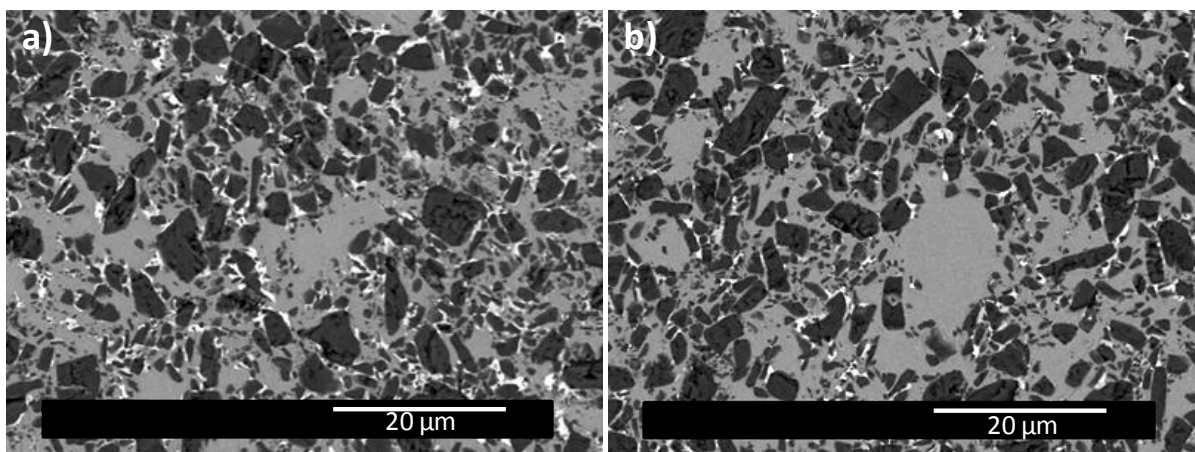


Figure 1. Microstructures (SEM images) of M2- Ti(C,N) cermet: a) as sintered, and b) heat treated

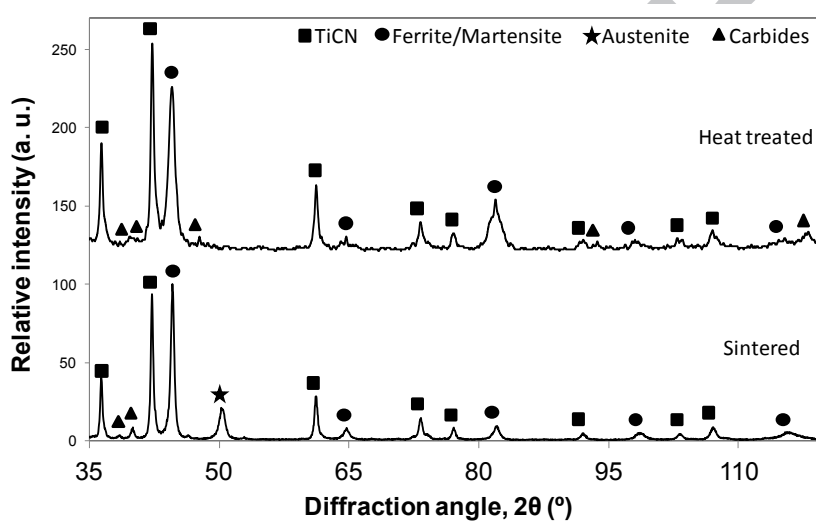


Figure 2. X-Ray Diffraction analysis of the M2- Ti(C,N) cermet as sintered and after heat treatment.

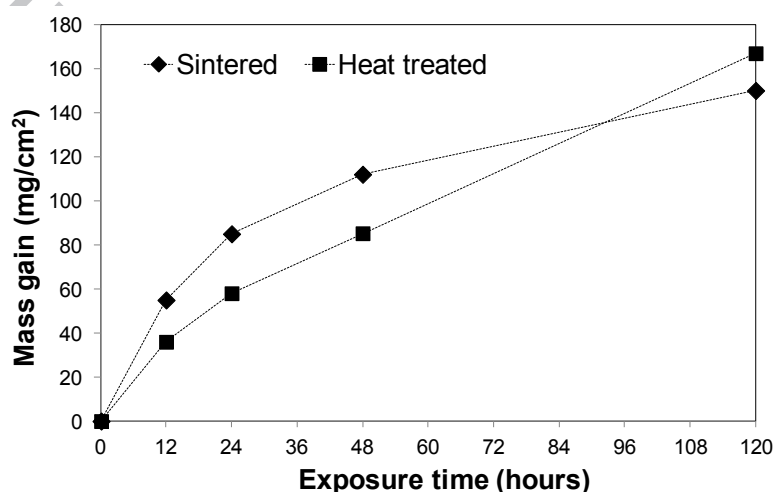


Figure 3. Mass gain with respect to the exposure time in oxidation tests at 1000 °C of the as-sintered and heat treated M2- Ti(C,N) cermet. (Experiments in furnace).

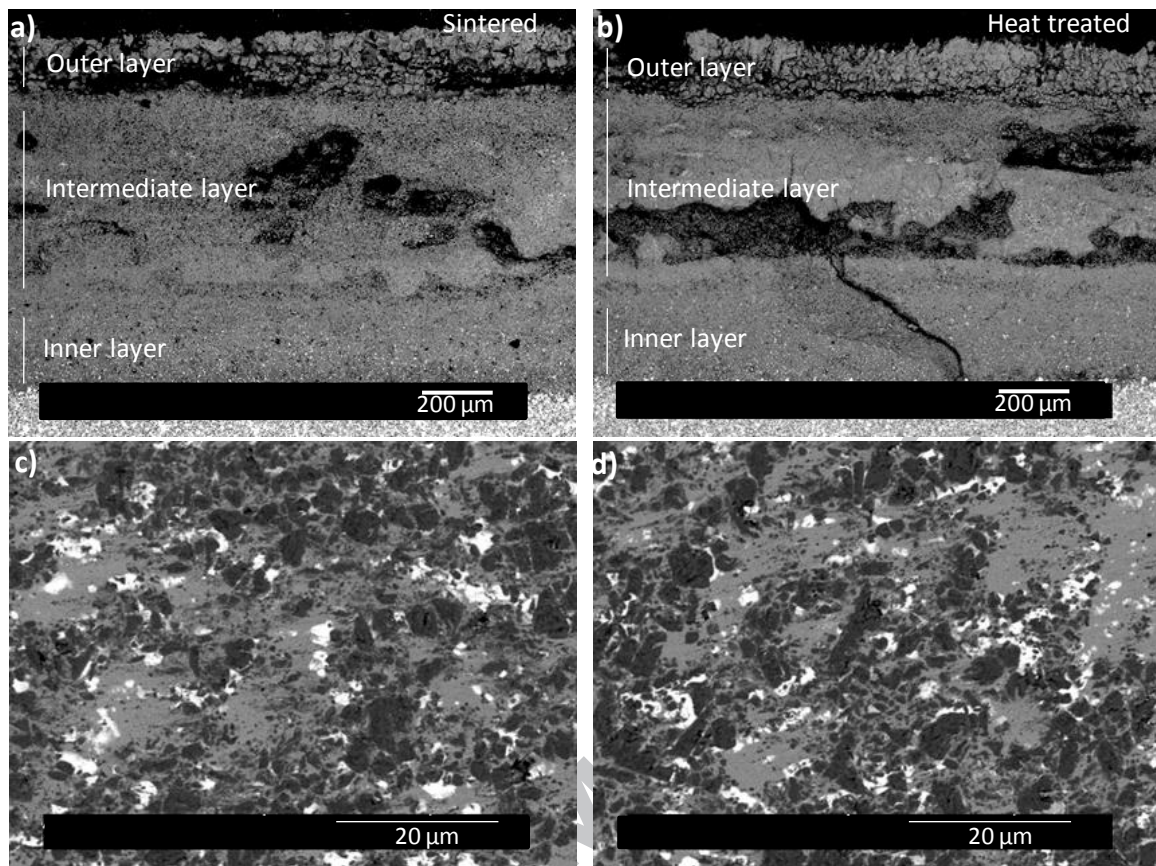


Figure 4. SEM images (BSE mode) of the cross section of the a) as-sintered and b) heat treated M2-Ti(C,N) cermet after the oxidation test at 1000 °C during 120 h. Detail of the bulk material after the oxidation experiment: c) as sintered, d) heat treated.

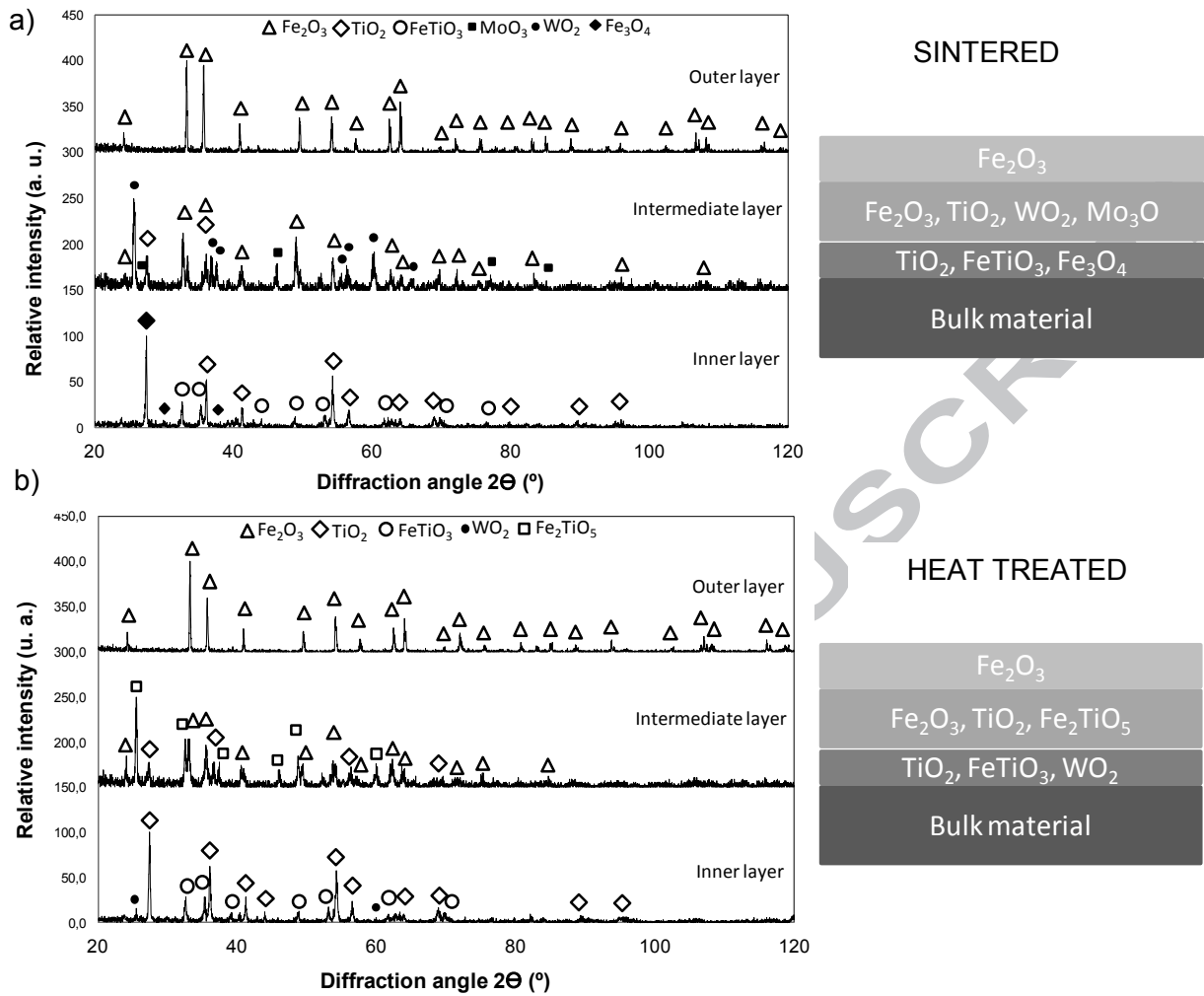


Figure 5. XRD analysis of the outer, intermediate and inner layers formed on the surface of the cermet M2-Ti(C,N) after the oxidation tests at 1000 °C during 120 h. a) As-sintered, b) heat treated.

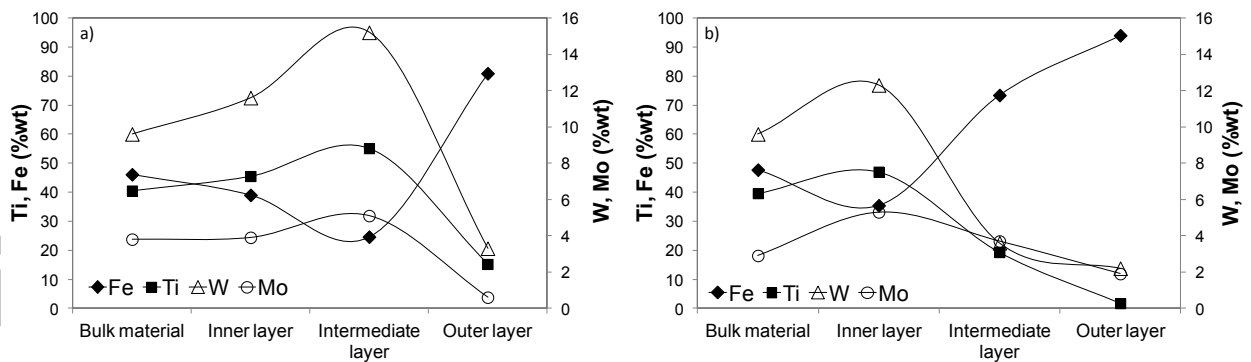


Figure 6. EDX analysis of surface layers of a) as-sintered and b) heat treated cermet.

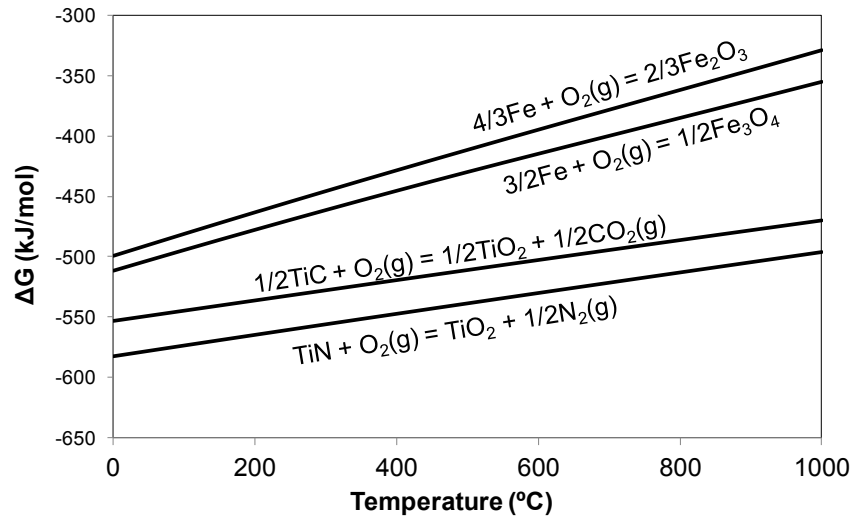


Figure 7. Gibbs standard free energy with respect to the temperature of the possible oxides formed during oxidation experiments, calculated by the software HSC 4.1.

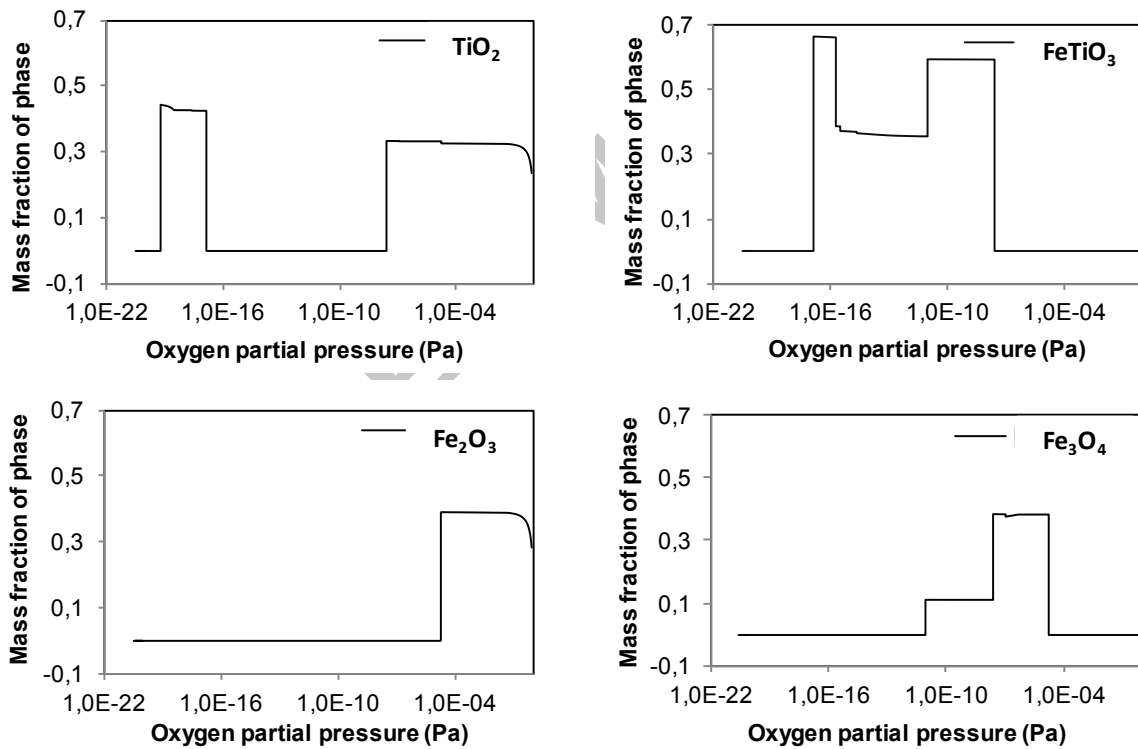


Figure 8. Phase fraction of a)  $\text{TiO}_2$ ; b)  $\text{FeTiO}_3$ ; c)  $\text{Fe}_2\text{O}_3$  and d)  $\text{Fe}_3\text{O}_4$  in the oxidation surface layers as a function of the oxygen partial pressure ( $P_{\text{O}_2}$ ) calculated with Thermocalc software [18].

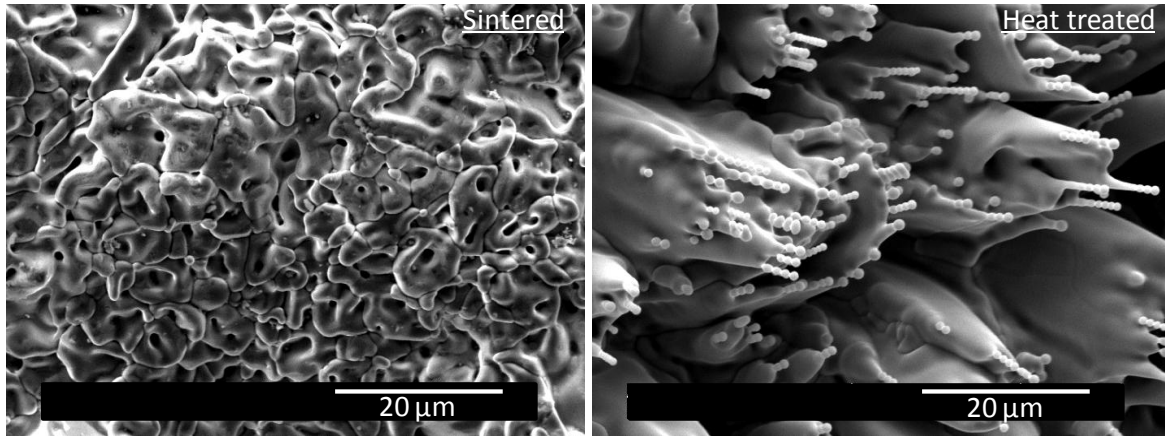


Figure 9. Morphology of the oxidation surface of as-sintered and heat treated cermet M2-Ti(C,N) after oxidation experiment at 1000 °C during 120 h in a muffle furnace.

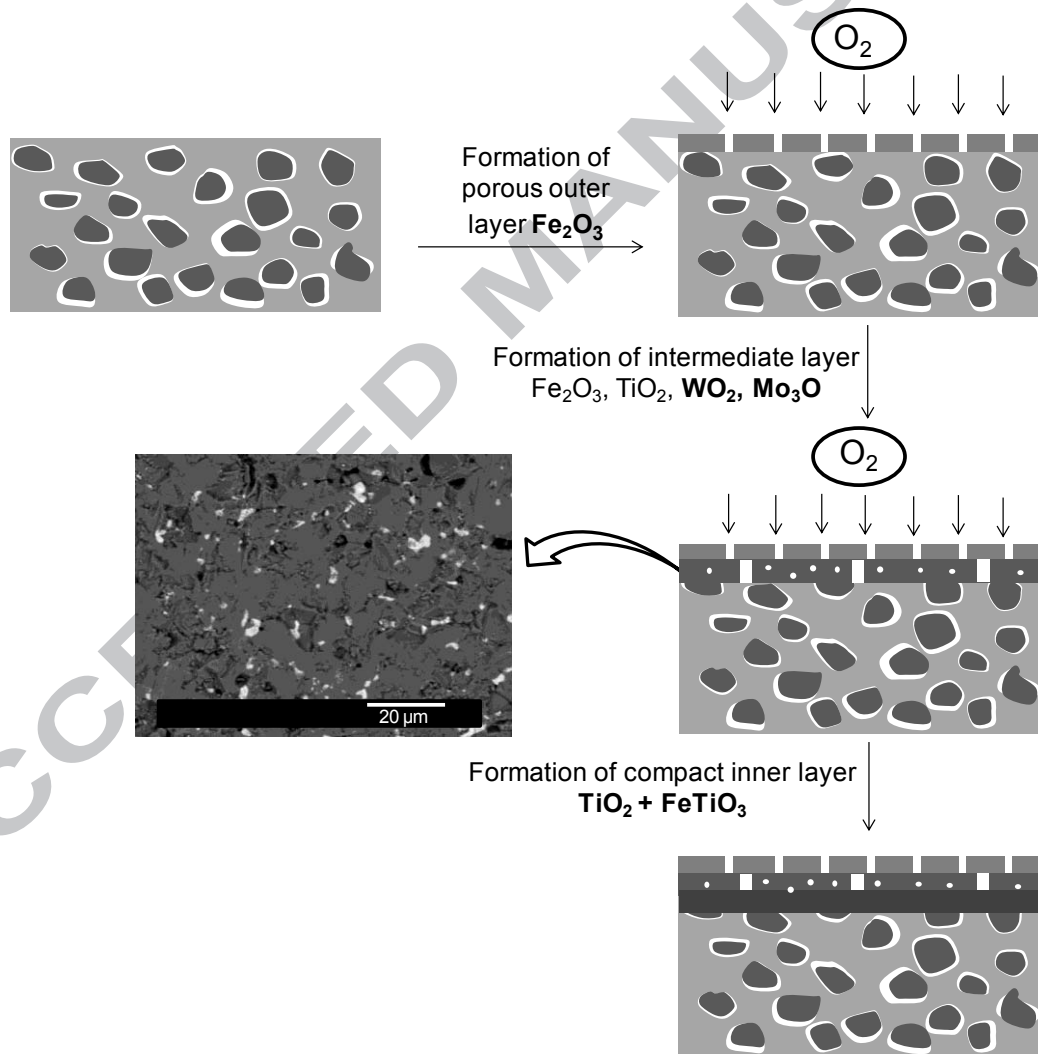


Figure 10. Schematic diagram of the oxidation mechanism proposed for the as-sintered cermet M2-Ti(C,N).

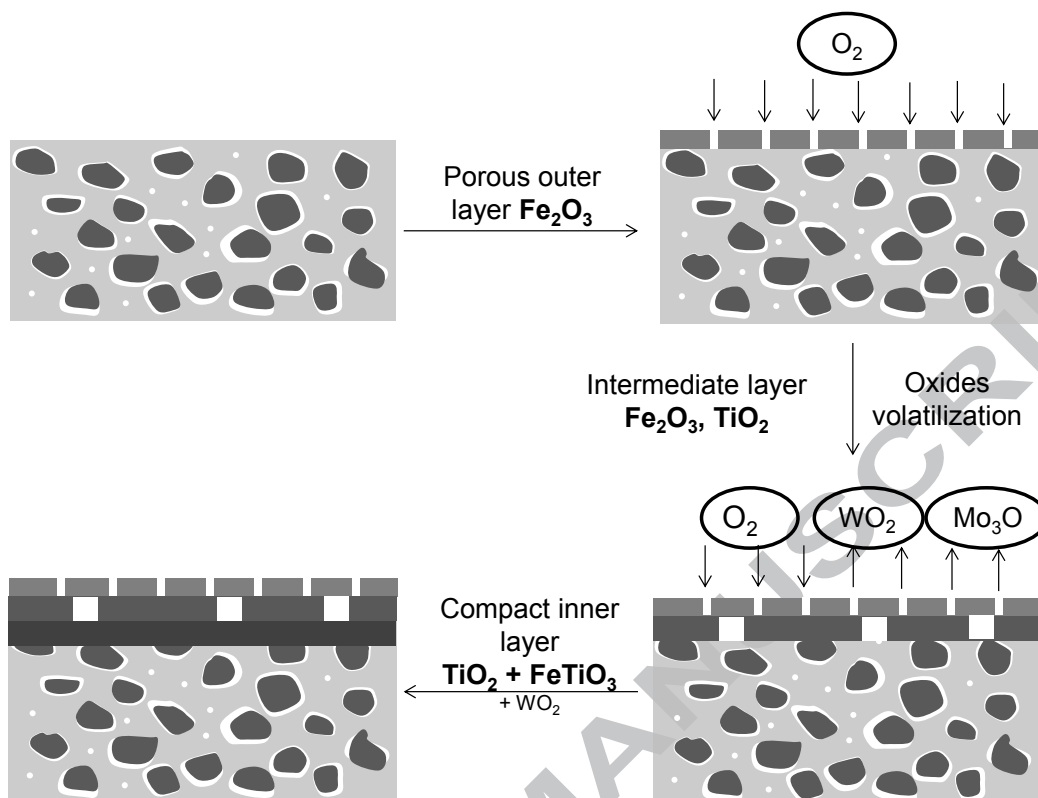


Figure 11. Schematic diagram of the oxidation mechanism proposed for the heat treated cermet M2-Ti(C,N).

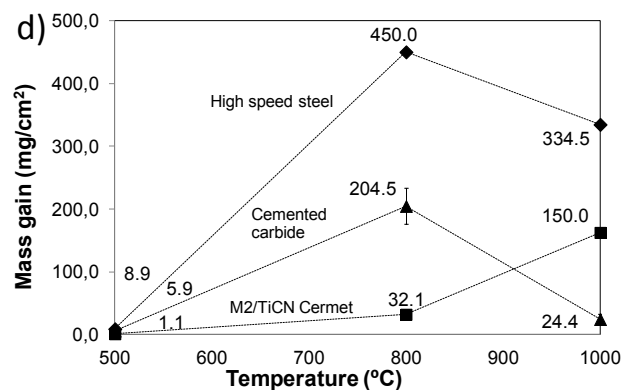
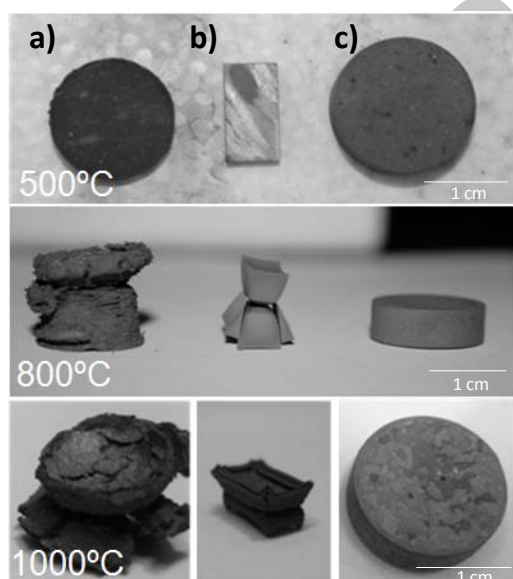


Figure 12. a) Samples of commercial M2 high speed steel, b) commercial hard metal and c) sintered M2-Ti(C,N) cermet after oxidation tests at 500 °C, 800 °C and 1000 °C during 120 h. d) Mass gain of commercial M2 high speed steel, commercial hard metal and sintered M2-Ti(C,N) cermet respect to oxidation temperature in oxidation experiment performed in a muffle furnace during 120 h.

**Highlights**

- Oxidation behavior study of a new steel matrix TiCN-based cermet
- Higher oxidation resistance of the cermet than commercial materials.
- High oxidation resistance due to the formation of a  $\text{TiO}_2$  and  $\text{FeTiO}_3$  protective layer.
- Oxidation mechanisms are proposed to explain the oxidation behavior.

## Graphical abstract

